

Nanowire Gold Chains: Formation Mechanisms and Conductance

Hannu Häkkinen, Robert N. Barnett, Andrew G. Scherbakov, and Uzi Landman*

School of Physics, Georgia Institute of Technology, Atlanta, Georgia 30332-0430

Received: July 22, 2000

Structural transformations, electronic spectra, and ballistic transport in pulled gold nanowires are investigated with *ab initio* simulations, and correlated with recent measurements. Strain-induced yield of an initial double-strand wire results first in formation of a bent chain which transforms upon further elongation to a linear atomic chain exhibiting dimerized atomic configurations. These structures are stabilized by directional local bonding with *spd* hybridization. The conductance of the initial double-stranded contact is close to $2(2e^2/h) \equiv 2g_0$, and it drops sharply to $1g_0$ during the transformation to a single chain, exhibiting subsequently a $\sim 1g_0$ plateau extending over an elongation well above typical Au–Au distances.

Generation of nanometer-scale crystalline wires (NWs) through elongation of materials' contacts had been predicted via early molecular dynamics simulations,¹ and their mechanical, structural, and electrical properties have been the subject of intensive investigations² owing to increasing basic and technological interest in such NWs. Most recently,³ high-resolution electron microscope (HRTEM) images, recorded during retraction of a tip from a gold surface, portrayed the development of a sequence of crystalline NW structures made of parallel atomic strands oriented along the NW axis, with the number of strands decreasing one-by-one, culminating in a one-atom wide and four-atom long linear chain of Au atoms.^{3,4} Furthermore, the simultaneously measured conductance revealed³ a staircase of quantized values (close to integer multiples of the conductance quantum $g_0 = 2e^2/h$) with the disappearance of each atomic strand, coinciding at the final pulling stages with an approximate unit (g_0) drop in the measured conductance. These experiments stimulated recent electronic structure calculations pertaining to single-chains of gold atoms.^{5–8}

Aiming at elucidation of the atomic-scale structural evolution and transformation mechanisms, and of bonding and transport characteristics at the ultimate stages of elongation of gold NWs, we report here results from large-scale *ab initio* density functional simulations^{9,10} in conjunction with conductance calculations.¹¹ Our findings reveal that the formation mechanism of a four-atom long single-chain NW, generated through straining of a double-strand (ds) wire (see bottom left configuration in Figure 1a), involves stress accumulation followed by eventual yield of one of the atomic strands, with the consequent atomic rearrangement resulting first in a (lower-energy) bent-chain (bc) configuration (top left configuration in Figure 1a). The yield event is accompanied by a significant decrease in the pulling force and a sharp drop in the conductance to $1g_0$ (see top in Figure 1a). Further separation of the two electrodes results in a transformation to a linear-chain (lc) structure (see right configuration in Figure 1a), with continued elongation leading to formation of dimerized configurations. Initial dimerization develops between the inner atoms of the wire (i.e., inner dimerization, id), transforming at a later stage to one where each of the inner atoms pairs with an end atom of the chain (i.e.,

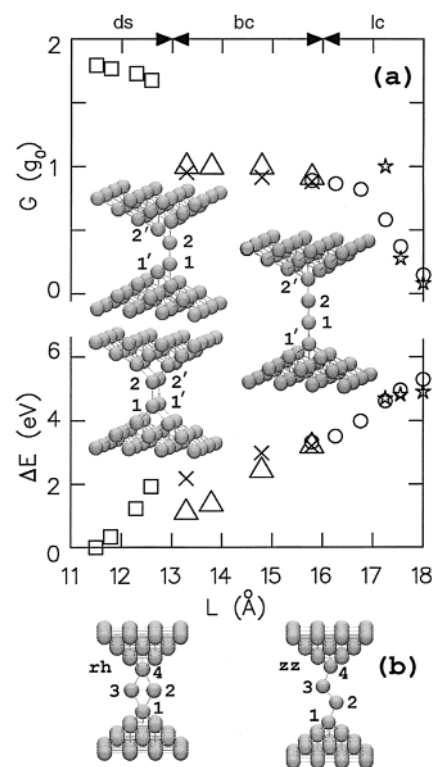


Figure 1. (a) Energies (ΔE , in units of eV plotted at the bottom, relative to the initial ds configuration at $L = 11.5 \text{ \AA}$) and conductances (G , in units of g_0 , plotted at the top) of Au NWs versus the distance between the outermost layers of the opposing electrodes, L ; the double-strand (ds, squares), bent-chain (bc, triangles), and linear-chain (lc, circles) intervals are marked at the top. The values for the rhombic (rh) isomer at $L = 13.3 \text{ \AA}$ and for the zigzag (zz) isomers at $L = 14.8$ and 15.8 \AA are marked by crosses, and those for the end-dimer configurations at $L = 17.3$, 17.6 , and 18 \AA are depicted by stars. The elongation force between consecutive structures may be estimated by the corresponding slope $\Delta E/\Delta L$. The atomic configurations (with atom indices) shown as insets to (a) correspond to the ds (left, bottom), bc (left, top), and lc (right) structures at $L = 12.6$, 13.3 , and 16.3 \AA respectively. (b) Atomic configurations for the rh isomer at $L = 13.3 \text{ \AA}$ ($d(1,2) = 2.76 \text{ \AA}$, $d(2,3) = 2.59 \text{ \AA}$, and $\angle(1,2,4) = 124^\circ$), and for the zz isomer at $L = 14.8 \text{ \AA}$ ($d(1,2) = d(3,4) = 2.55 \text{ \AA}$, $d(2,3) = 2.52 \text{ \AA}$ and $\angle(1,2,3) = 119^\circ$).

* Corresponding author.

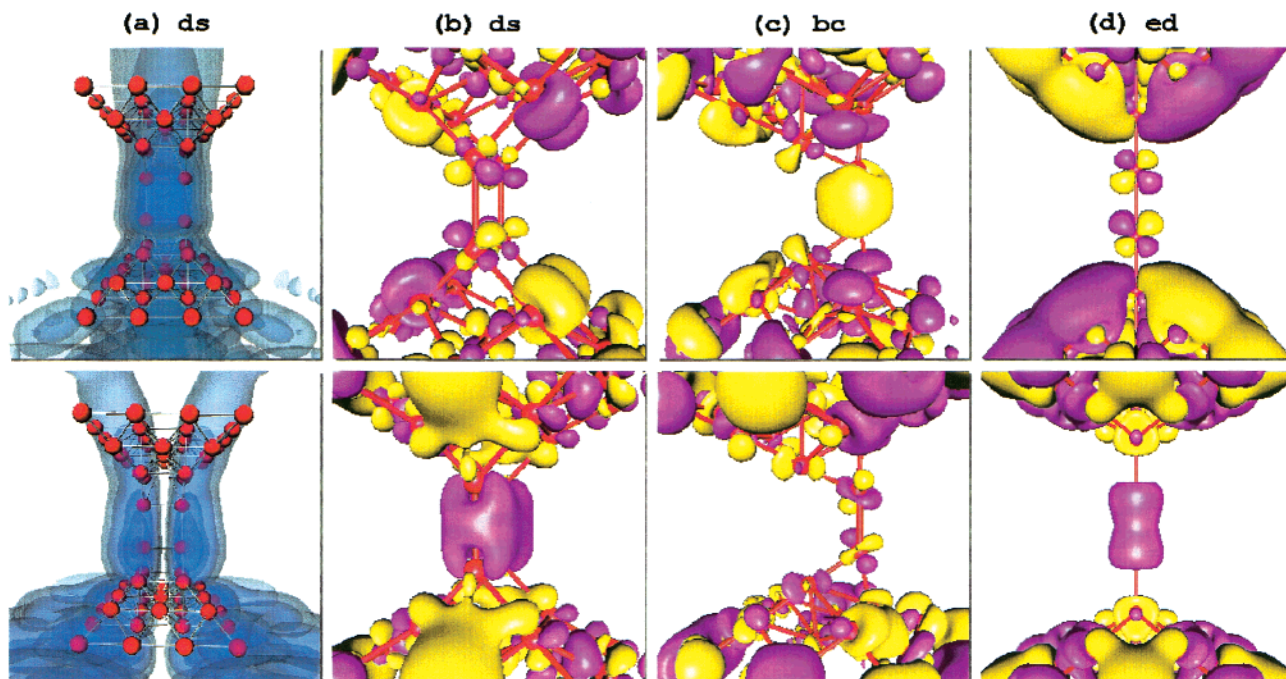


Figure 2. (a) Iso-surface images of the magnitudes of the first ($0.97g_0$, top) and second ($0.7g_0$, bottom) transmitted eigenchannels for the highly strained ds configuration (at $L = 12.6$ Å). (b and c) HOMO (top) and HOMO(-1) (bottom) orbitals corresponding to the highly strained ds NW (in b) and to the bc configuration at $L = 13.3$ Å (in c). (d) HOMO (top) and HOMO(-2) (bottom) orbitals for the ed configuration at $L = 17.3$ Å. In (a–d) Au atoms are depicted by red spheres. In (a) we display the entire atomic system including parts of the jellium-slab continuations of the electrodes (used in the conductance calculations), and in (b–d) we focus on the vicinity of the nanowires. The viewing orientation was chosen in each case to enhance visualization of the orbital characters on the wire atoms.

end-atom dimerization, ed). During the $ds \rightarrow bc \rightarrow lc$ evolution the conductance exhibits a $\sim 1g_0$ extended (4–4.5 Å long) plateau (see Figure 1a). The optimal structures determined here are stabilized by directional local bonding involving s, p, and d hybridization near the Fermi energy, and they are found to be energetically favorable to certain suggested alternative structural models.⁷

We start from a relaxed ds wire configuration with the distance between the two outermost layers of the opposing Au electrodes held at $L = 11.5$ Å; each of the electrodes is composed of 29 atoms arranged in 3 layers with face-centered-cubic (110) stacking in the z -direction (along the wire) and exposing {100} and {111} side facets. This crystallographic orientation, and the subsequent elongation process and conductance characteristics discussed below, correspond to experiments discussed in ref 3 and described in Figure 3 of that paper, where HRTEM and conductance measurements pertaining to gold nanowires created via controlled elongation of the contact between a tip and a (110) facet of a gold island are displayed. Note that this experiment is distinctly different from the one corresponding to Figure 4 of ref 3, which pertains to a wire formed through (spontaneous) thinning of a “nanobridge” connecting across a hole formed in a gold film by intense electron bombardment (in particular, unusually large interatomic distances of up to 3.5–4 Å were reported in ref 3 for the latter case, and *not* for the tip-pulling experiments which are the focus of our study).

In this initial configuration the 2-atom strands are parallel to each other, with almost equal inter- and intrastrand separations, $d_{\text{intra}}(1',2') = d_{\text{intra}}(1,2) = 2.66$ Å and $d_{\text{inter}}(1',1) = d_{\text{inter}}(2',2) = 2.67$ Å (see atom numbering in Figure 1a), and the distance between the topmost (interfacial) facets of the opposing electrodes is $d_{\text{el-el}} = 6.02$ Å. Note that all the distances involving atoms bridging the electrodes are smaller than the nn interatomic distance in bulk gold (2.885 Å), but larger than the bond-length

of the free Au_2 dimer (2.48 Å). The calculated conductance¹¹ of this configuration is $1.79g_0$.¹²

Elongation of the wire is simulated through increasing the separation between the outermost layers of the opposing electrodes (where the atoms are held at their fcc lattice positions with a lattice constant of bulk gold, 4.08 Å), followed by full relaxation of the system after each elongation step. The total elongation simulated here is $\Delta L = 6.5$ Å (using elongation increments of $0.25 \text{ Å} \leq \delta L \leq 1 \text{ Å}$, see Figure 1a), and we found that structural changes in response to increments in L involve mainly atoms forming the connective wire bridging the electrodes.

ds \rightarrow bc Transformation ($L \leq 13.3$ Å). Initial elongation results in higher-energy strained configurations with the pulling forces rising to ~ 4 nN (corresponding to the elongation increment from $L = 12.3$ to 12.6 Å, see Figure 1a), and it is accompanied by a gradual (small) decrease of the conductance to $G = 1.68g_0$ in the highly strained ds configuration shown at the bottom left in Figure 1a (corresponding to $L = 12.6$ Å with $d_{\text{el-el}} = 6.95$ Å).

For all the ds configurations the ballistic electron transport involves mainly two conductance eigenchannels (CCs), with the total conductance $G = g_0 \sum_n |\tau_n|^2$, where $0 \leq |\tau_n|^2 \leq 1$ is the transmission probability of the n th eigenchannel; for the initial ds configuration $|\tau_1|^2 = 0.99$, $|\tau_2|^2 = 0.76$, and for the highly strained one $|\tau_1|^2 = 0.97$ and $|\tau_2|^2 = 0.70$. The CCs are determined by quantization of the electron motion transverse to the propagation direction (z), due to the lateral confinement by the effective wire potential.^{10,11} Each of the transmitted CCs is found to be delocalized over the two atomic strands with the first CC being nodeless and the second having a nodal plane normal to the plane defined by the two strands and bisecting the interstrand Au–Au bonds (see Figure 2a); the delocalized nature of the CCs contrasts the conjecture³ that in such multi-

strand NWs each of the channels is associated with (and is confined about) an individual atomic strand implying two independent CCs connected in parallel to the electrodes.

The $ds \rightarrow bc$ elongation stage culminates in breaking of one of the strands, accompanied by displacements of each of the end atoms of the broken strand ($1'$ and $2'$ in Figure 1a) to the center of the underlying (110) rectangular facet of the corresponding electrode, yielding a lower-energy bc configuration, with a concomitant sharp drop in the conductance to $1g_0$ (see Figure 1a) involving a single CC. In the relaxed bc configuration (top left structure in Figure 1a) the end-to-end wire length $l_{ee} \equiv d(1',2') = 5.12 \text{ \AA}$, the distance between an interior atom to an nn end-atom of the wire $d_{ie} = d(1,1') = d(2,2') = 2.62 \text{ \AA}$, the bond length between the internal atoms of the wire $d_{ii} = d(1,2) = 2.56 \text{ \AA}$, and the bond angle $\angle(1',1,2) = 119^\circ$.

bc \rightarrow lc transformation ($13.3 \text{ \AA} \leq L \leq 16.3 \text{ \AA}$). During subsequent elongation, requiring initially a small pulling force ($\sim 0.8 \text{ nN}$, corresponding to the interval between $L = 13.3 \text{ \AA}$ and $L = 13.8 \text{ \AA}$), the bc wire straightens gradually resulting eventually (see right configuration in Figure 1a) in a linear chain at $L = 16.3 \text{ \AA}$.¹³ The $bc \rightarrow lc$ transformation spans an elongation range $\Delta L(bc \rightarrow lc) = 3.0 \text{ \AA}$, during which the conductance decreases only by about 10% (from $1g_0$ for the initial bc configuration to $0.87g_0$ for the lc one at $L = 16.3 \text{ \AA}$).

In light of a recent report pertaining to alternative structures for single-chain gold nanowires,⁷ we have explored such configurational isomers during the bc stage, with two of them shown in Figure 1b; a planar 4-atom rhombohedral (rh) arrangement at $L = 13.3 \text{ \AA}$ and a “zig-zag” (zz) structure at $L = 14.8 \text{ \AA}$. Energetically, these (relaxed) structural isomers are found to be local minima with higher energies (and slightly lower conductance) than the corresponding bc configurations (see Figure 1a). The zz isomer and bc structure (as well as the lc) become approximately degenerate at $L = 15.8 \text{ \AA}$, and upon further elongation (i.e., for $L = 16.3 \text{ \AA}$) both the zz and the bc convert to a linear chain. Note that although all these isomers (rh , zz , bc , lc) are found to be local minima for a free Au_4 cluster, the energetic ordering of structural isomers observed here for the four-atom NW cannot be deduced from that of the free cluster.¹⁴

lc \rightarrow Breaking ($L \geq 16.3 \text{ \AA}$). With continued pulling, the lc wire shows a tendency toward dimerization. At first (for $16.3 \leq L \leq 17.3 \text{ \AA}$) the only stable structures correspond to internal dimerization (id) of the wire, with $d_{ii} < d_{ie}$.¹⁵ At the start of this elongation interval, the conductance decreases only slightly, with a marked drop at $L = 17.3 \text{ \AA}$. However, starting at $L = 17.3 \text{ \AA}$ an energetically competitive dimerization mode of the lc wire emerges (being essentially degenerate with the id structure at 17.3 \AA) where $d_{ii} > d_{ie}$,¹⁶ with the conductance of this end-dimerized (ed) structure being $1g_0$. We note here (see Figure 1a) the markedly higher conductance of the ed structure ($G = 1g_0$) compared to that of the corresponding id chain.¹⁷ Such end-dimerized structures⁶ are energetically favored for the rest of the elongation process (that is for $L > 17.3 \text{ \AA}$).¹⁸ The force required for elongation during the end-dimerization stage is rather small (i.e., $\sim 0.3 \text{ nN}$ in the interval $17.6 \text{ \AA} \leq L \leq 18 \text{ \AA}$), and the conductance of the wire decreases sharply as eventual breaking is approached.

Throughout the structural evolution the electronic spectrum in the wire region is characterized by a dominant contribution of atomic d orbitals in the energy range $E_F - 4.5 \text{ eV} \leq E \leq E_F - 1 \text{ eV}$, with s , p , and spd hybrids contributing at energies above and below this range. Examination of the local densities of states reveals that the main variations in the spectrum in

response to the mechanical elongation occur predominantly in the interelectrode spatial region (the wire atoms, and the electrode atoms bound directly to them), involving mainly states in the vicinity of E_F .

To illustrate the nature of these states and their high sensitivity to structural variations we examine, for selected atomic configurations developed during the elongation process, orbital images (Figure 2b–d) and their angular-momentum decompositions about the wire atoms, corresponding to electronic states near E_F (i.e., highest occupied molecular orbitals, HOMO(j), with the index $j = -1, -2$ corresponding to the next-to-highest occupied orbitals in descending order). We observe that for the ds structure (see Figure 2b and the configuration shown at the bottom left in Figure 1a) the HOMO is of predominant d_{xz} character ($p_x^{0.2}d_{xz}^{0.76}$, here and in the following only the dominant m -components of p - and d -characters are given) and the HOMO(-1) is of strong sp_z character ($s^{0.34}p_z^{0.65}d_{z^2}^{0.12}$) on the strand atoms. These states evolve after the $ds \rightarrow bc$ transformation (see top left configuration in Figure 1a) into a HOMO with $s^{0.45}p_z^{0.50}(p_x^{0.25}p_z^{0.25}d_{xz}^{0.32})$ on inner (end) atoms, and a HOMO(-1) with an almost pure (tilted) d_{z^2} character on the inner atom ($p_x^{0.03}d_{z^2}^{0.9}$) and a ($s^{0.5}p_x^{0.08}d_{x^2-y^2}^{0.32}$) hybrid on the end atoms of the bent chain (Figure 2c).

The structural evolution during the $bc \rightarrow lc$ stage and the formation of dimerized configurations of the lc are accompanied by reordering of the orbitals near E_F with the HOMO orbital on the inner atoms of the wire acquiring a predominant ($p_x^{0.03}d_{xz}^{0.95}$) d_{xz} character (see, e.g., Figure 2d corresponding to the ed configuration); as evident the d_{xz} components on the two inner atoms of the ed wire combine locally in an antibonding manner, while in the (lower-energy) HOMO(-1) orbital (not shown) they are in a local bonding orientation with respect to each other. The HOMO(-2) orbital (Figure 2d) of the ed configuration is characterized by a strong s character on the inner-atoms ($s^{0.86}p_z^{0.11}d_{z^2}^{0.03}$) combining to form a σ -like local bond, and an sd hybridization on the end atoms of the chain ($s^{0.48}p_z^{0.06}d_{x^2-y^2}^{0.46}$).

The above hybridization patterns and in particular the strong contribution from d -orbitals to directional covalent-like bonding characteristics in the (interelectrode) wire region underlie and facilitate the structural transformation mechanism described by us, via stabilization of the sequence of strained atomic configurations which evolve in the elongation process. Consequently, formation of such (several atom long) single-chain nanostructures, reflected in an extended conductance plateau (with close to unit conductance) before breaking⁴ may not be found for materials where the above bonding patterns do not occur; indeed extended single chains were not observed (theoretically¹⁹ and experimentally⁴) for a simple metal contact (e.g., sodium).

Finally, we remark that the investigations presented here, which deepen our insights into the structure, formation mechanism, and conductance of atomic double-strand and single-strand nanocontacts between gold electrodes, pertain to the type of tip-pulling experiments reported in the *first* part of ref 3 (see Figure 3 in ref 3), and they are *not* aimed at explaining the extraordinary stability of monatomic thick wires bridging two sections of a suspended thin gold film, where interatomic distances up to $3.5\text{--}4 \text{ \AA}$ were reported from HRTEM images (see the *second* part of ref 3, particularly Figure 4 therein). Indeed, the formation of wires in the latter experiments involves an initial intense electron bombardment to perforate holes in the film and subsequent thinning of the formed “nanobridges” driven by stress and strain relaxation processes; additionally,

the nature of such experiments differs greatly from the controlled tip-pulling experiments, on which we focus here. We remark that none of the theoretical studies reported to date^{5–8} have been able to consistently explain the abovementioned anomalously long interatomic distances in the nanobridges,²⁰ indicating that new theoretical considerations are needed, including examinations of possible effects caused by light impurity atoms, which while affecting the structure of the nanowire may not have enough contrast to be visible in HRTEM images.²¹

Acknowledgment. This research is supported by the U.S. DOE and the Academy of Finland. Calculations were performed on an IBM SP2 at the Georgia Tech Center for Computational Materials Science, and on a Cray T3E at the National Energy Research Scientific Computing Center (NERSC) at Berkeley, CA.

References and Notes

- (1) Landman, U.; Luedtke, W. D.; Burnham, W. A.; Colton, R. J. *Science* **1990**, *248*, 454. Landman, U.; Luedtke, W. D. *J. Vac. Sci. Technol.* **1991**, *B9*, 414.
- (2) See, e.g., articles in: *Nanowires*, Serena, P. A., Garcia, N., Eds.; Kluwer: Dordrecht, 1997.
- (3) Ohnishi, H.; Kondo, Y.; Takayanagi, K. *Nature* **1998**, *395*, 780.
- (4) For a report on formation of single-chain Au NWs, inferred from observations of an extended $1g_0$ conductance plateau, see: Yanson, A. I.; Rubio Bollinger, G.; van der Brom, H. E.; Agraït, N.; van Ruitenbeek, J. M. *Nature* **1998**, *395*, 783.
- (5) Torres, J. A.; Tosatti, E.; Dal Corso, A.; Ercolessi, F.; Kohanoff, J. J.; Di Tolla, F. D.; Soler, J. M. *Surf. Sci.* **1999**, *426*, L441.
- (6) Okamoto, M.; Takayanagi, K. *Phys. Rev. B* **1999**, *60*, 7808. In this study only s-electrons were included.
- (7) Sánchez-Portal, D.; Artacho, E.; Junquera, J.; Ordejón, P.; García, A.; Soler, J. M. *Phys. Rev. Lett.* **1999**, *83*, 3884.
- (8) De Maria, L.; Springborg, M. *Chem. Phys. Lett.* **2000**, *323*, 293. The statement made in this paper that the studies in refs 7 (D. Sánchez-Portal et al.) and 10 (H. Häkkinen et al.) did not include relativistic effects is erroneous.
- (9) The calculations were performed using the ab initio Born–Oppenheimer (BO) local-spin-density (LSD) molecular dynamics method (BO-LSD-MD, for details see: Barnett, R. N.; Landman, U. *Phys. Rev. B* **1993**, *48*, 2081. The $5d^{10}6s^1$ valence electrons of a gold atom are described by scalar-relativistic norm-conserving nonlocal pseudopotentials (Troullier, N.; Martins, J. L. *Phys. Rev. B* **1991**, *43*, 1993) with a plane-wave basis set (kinetic energy cutoff of 62 Ry). See also: Häkkinen, H.; Barnett, R. N.; Landman, U. *Phys. Rev. Lett.* **1999**, *82*, 3264 and ref 10.
- (10) A preliminary discussion pertaining to the inner-dimerized linear-chain configuration and the adsorption of a methanethiol to it can be found in: Häkkinen, H.; Barnett, R. N.; Landman, U. *J. Phys. Chem. B* **1999**, *103*, 8814.
- (11) In calculations of the conductance we used a recursion-transfer-matrix method (see: Hirose K.; Tsukada, M. *Phys. Rev. B* **1995**, *51*, 5278). In this method the transmission of an electron propagating from one electrode to the other through the LDA self-consistent effective potential of the connected nanowire, calculated for each of the relaxed wire configurations and processed according to the procedure described in: Nakamura, A.; Brandbyge, M.; Hansen, L. B.; Jacobsen, K. W. *Phys. Rev. Lett.* **1999**, *82*, 1538, is evaluated using a numerical solution for the stationary states to the Schrödinger equation with scattering boundary conditions. Inside the electrodes, i.e., away from the wire/electrode contact region the effective potential converges to a constant value which is then used to represent the continuation of the electrodes. The solution is achieved via discretization of the Schrödinger equation in slices along the wire axis and using periodic boundary conditions in the transverse directions. Transfer-matrix recursion formalism is used to propagate the solution from one slice to the adjacent one starting from the constant-potential region in one of the electrodes and propagating through the wire into the constant-potential region of the receiving electrode. In these conductance calculations 512 plane waves were used to achieve convergence. Transformation to nonmixing eigenchannels was performed following: Brandbyge, M.; Sørensen, M. R.; Jacobsen, K. W. *Phys. Rev. B* **1997**, *56*, 14956.
- (12) For a relaxed longer ds wire (i.e., two 4-atom-long strands with $d_{\text{inter}} = 2.59 \text{ \AA}$, $d_{\text{intra}} = 2.73 \text{ \AA}$, and $d_{\text{el-el}} = 11.73 \text{ \AA}$), we obtained $G = 1.97g_0$.
- (13) In the lc configuration at $L = 16.3 \text{ \AA}$ and $l_{\text{ee}} = 7.94 \text{ \AA}$, $d_{\text{ie}} = 2.66 \text{ \AA}$, and $d_{\text{ii}} = 2.62 \text{ \AA}$.
- (14) The same LDA calculations (ref 9) for the free Au₄ cluster show that the ground state is a planar rhombus (rh) with $d(1,2) = 2.70 \text{ \AA}$ and $\angle(1,2,4) = 121^\circ$. The zz isomer with $d(1,2) = d(3,4) = 2.55 \text{ \AA}$, $d(2,3) = 2.60 \text{ \AA}$ and $\angle(1,2,3) = 130^\circ$ (see atom numbering in Figure 1b for rh and zz) is of higher energy ($\Delta E = 0.84 \text{ eV}$), and the lc isomer, with $d(1,2) = d(3,4) = 2.52 \text{ \AA}$ and $d(2,3) = 2.59 \text{ \AA}$, is of even higher energy ($\Delta E = 1.34 \text{ eV}$). A bc isomer ($d(1,2) = d(3,4) = 2.51 \text{ \AA}$, $d(2,3) = 2.61 \text{ \AA}$, and $\angle(1,2,3) = 126^\circ$) is found to be the highest in energy ($\Delta E = 1.40 \text{ eV}$).
- (15) For $L = 16.3 \text{ \AA}$ see ref 13, and for $L = 17.3 \text{ \AA}$ and $l_{\text{ee}} = 8.82 \text{ \AA}$, $d_{\text{ii}} = 2.68 \text{ \AA}$, and $d_{\text{ie}} = 3.07 \text{ \AA}$.
- (16) For the ed structure at $L = 17.3 \text{ \AA}$ and $l_{\text{ee}} = 8.75 \text{ \AA}$, $d_{\text{ii}} = 3.31 \text{ \AA}$, and $d_{\text{ie}} = 2.72 \text{ \AA}$.
- (17) The significantly smaller conductance of the id configuration at $L = 17.3 \text{ \AA}$ (see Figure 1a) is caused by narrowing of the potential profile in the regions between the internal dimer atoms and the end-atoms of the chain (see Figure 4a in ref 10), with the consequent reduced coupling between the inner dimer atoms and the electrodes, resulting in enhanced backscattering of the incident electron from these “bottleneck” regions. Note that at finite temperature fluctuations between the essentially degenerate id and ed structures may occur leading to sizable noise in the measured conductance ($G \sim 0.6 - 1g_0$) at the final stages of elongation.
- (18) At $L = 17.6 \text{ \AA}$ and $l_{\text{ee}} = 9.34 \text{ \AA}$, $d_{\text{ii}} = 4.24 \text{ \AA}$, $d_{\text{ie}} = 2.55 \text{ \AA}$, and at $L = 18 \text{ \AA}$ and $l_{\text{ee}} = 9.81 \text{ \AA}$, $d_{\text{ii}} = 4.75 \text{ \AA}$, and $d_{\text{ie}} = 2.53 \text{ \AA}$.
- (19) Barnett, R. N.; Landman, U. *Nature* **1997**, *387*, 788. Häkkinen, H.; Manninen, M. *Europhys. Lett.* **1998**, *44*, 80.
- (20) In ref 7 it was suggested that experimentally observed linear wires with long interatomic distances would in fact consist of spinning “zigzag” structures having typical Au–Au nearest-neighbor distances, but with only the atoms on the rotation axis visible in HRTEM. However, in such structures even the spinning off-axis atoms should generate enough contrast to be clearly visible for imaging (Ugarte, D., private communication).
- (21) For instance, while it is well-known that oxygen does not adsorb molecularly on bulk gold, it may interact more strongly with the formed nanobridges of the film, and may even dissociate due to heating/strain effects in the film. Atomic oxygen binds strongly on small gold clusters with typical O–Au distance of $1.9 - 2.1 \text{ \AA}$ (Häkkinen, H., unpublished data). Linear chains of alternating Au and O atoms (provided that they would be stable as suspended chains) would thus have Au–Au distances of $\approx 4 \text{ \AA}$. For a discussion of related chemical adsorption effects on the structure and electric transport properties of gold nanowires see ref 10.